[4] Takumida M, Popa R, Anniko M. Free radicals in the guinea pig inner ear following gentamicin exposure. ORL J Otorhinolaryngol Relat Spec 1999;61:63–70.
[5] Levine JD, Alessandri-Haber N. TRP channels: targets for the relief of pain. Biochim Biophys Acta 2007;1772:989–1003.
[6] Bauer CA, Brozoski TJ, Myers KS. Acoustic injury and TRPV-1 expression in the cochlear spiral ganglion. Int Tinnitus J 2007;13:21–8.
[7] Shin J, Cho H, Hwang SW, Jung J, Shin CY, Lee SY, et al. Bradykinin-12-lipoxygenase-VR1 signaling pathway for inflammatory hyperalgesia. Proc Natl Acad Sci USA 2002;99:10150–5.
[8] Stucky CL, Abrahams LG, Seybold VS. Bradykinin increases the proportion of neonatal rat dorsal root ganglion neurons that respond to capsaicin and protons. Neuroscience 1998;84:1257–65.
[9] Veldhuis WB, van der Stelt M, Wadman MW, van Zadelhoff G, Maccarrone M, Veldink GA, et al. Neuroprotection by the endogenous cannabinoid anandamide and arvanil against in vivo excitotoxicity in the rat: role of vanilloid receptors and lipoxygenases. J Neurosci 2003;23:4127–33.
[10] Winter J. Brain derived neurotrophic factor, but not nerve growth factor, regulates capsaicin sensitivity of rat vagal ganglion neurons. Neurosci Lett 1998;241:21–4.
[11] Zheng JL, Stewart RR, Gao W-Q. Neurotrophin-4/5, brain-derived neurotrophic factor, and neurotrophin-3 promote survival of cultured vestibular ganglion neurons and protect them against neurotoxicity of ototoxins. J Neurobiol 1995;28:330–40.
[12] Takumida M, Anniko M. Brain-derived neurotrophic factor and nitric oxide synthase inhibitor protect the vestibular organ against gentamicin ototoxicity. Acta Otolaryngol 2002;122:10–5.
[13] Hegarty JL, Kay AR, Green SH. Trophic support of cultured spiral ganglion neurons by depolarization exceeds and is additive with that by neurotrophins or cAMP and requires elevation of [$Ca2^+$]i within a set range. J Neurosci 1997;17:1959–70.
[14] Hansen MR, Zha XM, Bok J, Green SH. Multiple distinct signal pathways, including an autocrine neurotrophic mechanism, contribute to the survival-promoting effect of depolarization on spiral ganglion neurons in vitro. J Neurosci 2001;21:2256–67.
[15] Shimosato G, Amaya F, Ueda M, Tanaka Y, Decosterd I, Tanaka M. Peripheral inflammation induces up-regulation of TRPV-2 expression in rat DRG. Pain 2005;119:225–32.
[16] Tamura S, Morikawa Y, Senba E. TRPV-2, a capsaicin receptor homologue, is expressed predominantly in the neurotrophin-3-dependent subpopulation of primary sensory neurons. Neuroscience 2005;130:223–8.
[17] Tabuchi K, Suzuki M, Mizuno A, Hara A. Hearing impairment in TRPV-4 knockout mice. Neurosci Lett 2005;382:304–8.
[18] Lipski J, Park TIH, Li D, Lee SCW, Trevarton AJ, Chung KKH, et al. Involvement of TRP-like channels in the acute ischemic response of hippocampal CA1 neurons in brain slices. Brain Res 2006;1077:187–99.
[19] Takeda-Nakazawa H, Harada N, Shen J, Kubo N, Zenner H-P, Yamashita T. Hypotonic stimulation-induced nitric oxide production in outer hair cells of the guinea pig cochlea. Hear Res 2007;227:59–70.
[20] Roehm P, Hoffer M, Balaban CD. Gentamicin uptake in the chinchilla inner ear. Hear Res 2007;230:43–52.

Acta Oto-Laryngologica, 2010; 130: 1278–1286

informa
healthcare

ORIGINAL ARTICLE

Expression of transient receptor potential channel vanilloid (TRPV) 1–4, melastin (TRPM) 5 and 8, and ankyrin (TRPA1) in the normal and methimazole-treated mouse olfactory epithelium

YOUSUKE NAKASHIMO[1], MASAYA TAKUMIDA[1], TAKASHI FUKUIRI[1], MATTI ANNIKO[2] & KATSUHIRO HIRAKAWA[1]

[1]*Department of Otolaryngology, Hiroshima University Faculty of Medicine, Hiroshima, Japan and* [2]*Department of Otolaryngology, Head and Neck Surgery, University Hospital, Uppsala, Sweden*

Abstract

Conclusion: It is suggested that TRPV1, 2, 3, and 4, TRPM5 and 8, and TRPA1 may play several roles in the olfactory epithelium (OE), contributing to olfactory chemosensation, olfactory adaptation, olfactory–trigeminal interaction, and OE fluid homeostasis. In patients with olfactory disturbance, TRPV1 and TRPM8 may be closely related to a high rate of recognition of curry and menthol odors, while TRPV2 may also play a crucial role in the regeneration of olfactory receptor neurons. *Objective:* Expression of TRPV1–4, TRPM5 and 8, and TRPA1 in the normal and methimazole-treated mouse OE was analyzed. *Methods:* The localization of TRPV1–4, TRPM5 and 8, and TRPA1 in the OE of normal and methimazole-treated CBA/J mice was investigated by immunohistochemistry. *Results:* Normal OE showed a positive immunofluorescent reaction to TRPV1–4, TRPM5 and 8, and TRPA1. In lamina propria, the nerve fibers displayed TRPV 1, 2, and 3, TRPM8 and TRPA1. In the pathological condition, the expression of TRPV3, TRPV4, TRPM5, and TRPA1 was markedly reduced and took a long time to recover. In contrast, expression of TRPM8 was scarcely affected, even in the pathological condition, while TRPV1 and TRPV2 showed early recovery following methimazole treatment.

Keywords: *Immunohistochemistry, olfactory chemosensation, olfactory disturbance*

Introduction

The TRP (transient receptor potential) ion channel family comprises 28 channels, divided into 6 subgroups according to their structure and activation characteristics. TRP subfamilies include canonical (TRPC, seven channels), melastatin (TRPM, eight), ankyrin (TRPA, one), vanilloid (TRPV, six), polycystin (TRPP, three), and mucolipin (TRPML, three channels). TRP channels play a crucial role in the responses to all major classes of external stimuli, including light, sound, chemicals, temperature, and touch. TRP channels also imbue individual cells with the ability to sense changes in the local environment, such as alterations in osmolality [1].

Thermosensing can be considered the most elementary of all senses, as it is absolutely crucial for our survival. A prompt reaction to contact with harmfully cold or hot objects is vital to prevent acute, potentially fatal, injury. Moreover, to maintain the core body temperature of around 37°C, heat production and heat loss must be maintained equal in steady state. This requires the permanent monitoring and integration of thermal information from the skin (via peripheral thermoreceptors) and deep body structures (via central thermoreceptors), and the ensuing initiation of reflexes that promote heat production or heat loss.

Recent studies have provided the first molecular insight into the mechanisms underlying the exquisite thermo- and chemosensitivity of these channels.

Correspondence: Yousuke Nakashimo MD, Department of Otolaryngology, Hiroshima University Faculty of Medicine, 1-2-3 Kasumi, Minamiku, Hiroshima 734-8551, Japan. E-mail: yosabnm1@hiroshima-u.ac.jp

(Received 17 March 2010; accepted 21 March 2010)

ISSN 0001-6489 print/ISSN 1651-2251 online
DOI: 10.3109/00016489.2010.489573

Moreover, accumulating evidence implicates TRP channels in the development of the central nervous system. A superfamily subset of TRPs, dubbed thermo-TRPs, are highly sensitive to temperature, and several of them serve essentially as molecular thermometers in different cell populations of the peripheral sensory system [2].

In the olfactory epithelium (OE), expression of several TRP channels has been reported. Recent investigations revealed the expression of TRPVs and a possible functional role in the OE [3,4], TRPV1–4 variably with a diffuse pattern in lamina propria, and in the respiratory epithelium, especially so in glandular cells of lamina propria. These findings suggested that TRPVs may play a variety of roles in the OE, contributing to olfactory adaptation, olfactory–trigeminal interactions in nasal chemoreception, and OE homeostasis; they may also be involved in olfactory transduction as well as olfactory dysfunction secondary to sinonasal inflammation disease [3]. However, the detailed distribution of TRPVs in the OE and the expression of other TRP channels in the OE, especially in pathological conditions, is still not known.

In this investigation we identified TRPV1–4 as well as TRPM5 and 8 and also TRPA1 in the OE in both normal and methimazole-treated mice. As these TRP channels are regarded as thermo-TRPs, it has recently been shown that temperature can influence olfaction [5].

Material and methods

We used 15 healthy, normal, 8-week-old CBA/J mice with body weights in the range 20–25 g. They were housed in a light-controlled room with a 12 h light/dark cycle and were allowed access to food and water ad libitum. Care and use of the animals was approved by the Animal Experimentation Committee, Hiroshima University School of Medicine (permit no. A08-88) and was in accordance with the Guide to Animal Experimentation, Hiroshima University and the guidelines of the Committee on Research Facilities for Laboratory Animal Science, Hiroshima University School of Medicine.

For the methimazole-treated study, 12 animals were injected intraperitoneally (i.p.) with 300 mg/kg methimazole dissolved in 2 ml of 0.01 M phosphate-buffered saline (PBS) containing 20% dimethyl sulfoxide (DMSO). These animals were used for the immunohistochemical study 1 day, 7 days, 4 weeks, and 3 months after the injection. The normal and methimazole-treated animals were deeply anesthetized with pentobarbital and fixed by cardiac perfusion with 4% paraformaldehyde in 0.1 M phosphate buffer solution, pH 7.4. Nasal tissue, including the OE, was excised and immersed in the same fixative for a further 1 h. It was decalcified with 0.1 M buffered Na-EDTA for 14 days. The specimens were cryoprotected in cold 20% sucrose in PBS, frozen in OCT mounting medium (Sakura Finetechnical Co. Ltd, Tokyo, Japan). Coronal sections were serially cut on a cryostat at 4 μm, and mounted on glass slides. After pretreatment with blocking serum, the specimens were incubated with a rabbit polyclonal antibody to TRPV1 (Transgenic Inc., Kumamoto, Japan) (diluted 0.1 μg/ml), rabbit polyclonal antibody to TRPV2 (abcam, Tokyo, Japan) (diluted 1:1000), goat polyclonal antibody to TRPV3 (Santa Cruz Biotechnology Inc, CA, USA) (diluted 1:50), a rabbit polyclonal antibody to TRPV4 (Alomone Labs Ltd, Jerusalem, Israel) (diluted 1:200), a goat polyclonal antibody to TRPM5 (Santa Cruz Biotechnology) (diluted 1:200), a rabbit polyclonal antibody to TRPM8 (Osenses Ltd) (diluted 1:300), or with a rabbit polyclonal antibody to TRPA1 (Transgenic) (diluted 1:200) in 0.3% Triton X-100-containing PBS at 4°C for 48 h. The specimens were then washed in PBS and incubated for 1 h with Alexa Fluor 488 goat anti-rabbit or donkey anti-goat secondary antibodies (1:500) (Molecular Probes, Eugene, OR, USA). The sections were washed and coverslipped with DakoCytomatia Fluorescent Mounting Medium (DakoCytomatia, CA, USA). The specimens were viewed in a Nikon fluorescence microscope (Eclipse E600) equipped with an appropriate filter set. Fluorescence analog images were obtained via an intensified digital color charge-coupled device camera (C4742-95; Hamamatsu Photonics) and stored as digital images using IP Lab Spectrum software (version 3.0; Signal Analytics Corp.). Appropriate controls with omission of the primary antibodies, or with specific blocking peptides of the primary antibodies, were included in the immunohistochemical protocol.

Measurement of fluorescence intensity

For the statistical analysis, we measured the fluorescence intensity in the olfactory receptor neurons (ORNs). ORNs were randomly selected from each specimen, and their fluorescence intensity was determined. The value of 10 cells was averaged for each specimen. The grand mean was obtained by averaging the means of six to eight specimens for normal and methimazole-treated animals. A standard error was calculated from the means for individual specimens. These data were analyzed by a two-way analysis of variance (ANOVA).

Results

Distribution of TRPV1–4, TRPM5, TRPM8, and TRPA1 in mouse OE

Under light microscopy, supporting cells, ORNs, and basal cells were readily identified by the shape and location of their nuclei. In lamina propria, nerve fibers, vessels, and Bowman's glands were observed.

TRPV1. In the OE, an immunofluorescent reaction to TRPV1 was observed in the ORNs, especially in dendrites and axons. Supporting cells and basal cells showed a weaker reaction to TRPV1. In lamina propria, nerve fibers and blood vessel walls were immunofluorescent.

TRPV2. An immunofluorescent reaction to TRPV2 was observed in the ORNs, especially in dendrites and axons. Basal cells were noticeably immunofluorescent, but supporting cells only weakly so. In lamina propria, nerve fibers were markedly immunofluorescent, while blood vessel walls and Bowman's glands were only moderately so.

TRPV3. An immunofluorescent reaction to TRPV3 was observed in the ORNs. Supporting cells and basal cells showed weaker immunofluorescence. In lamina propria, nerve fibers and blood vessel walls were weakly immunofluorescent.

TRPV4. An immunofluorescent reaction to TRPV4 was observed in the ORNs. Supporting cells and basal cells showed weak immunofluorescence to TRPV1. In lamina propria, TRPV4 labeling was comparatively weak and was absent altogether in nerve fibers.

TRPA1. The ORNs showed an immunofluorescent reaction to TRPA1. In lamina propria, Bowman's glands showed marked immunofluorescence, while the nerve fibers showed faint fluorescence.

TRPM5. ORNs were moderately immunofluorescent to TRPM5 and olfactory cilia were intensely immunofluorescent, while in the lamina propria, TRPM5 labeling was comparatively weak.

TRPM8. ORNs were intensely immunofluorescent to TRPM8 and olfactory cilia showed moderate immunofluorescence. Basal cells were also moderately immunofluorescent, but supporting cells revealed no fluorescence at all. In the lamina propria, nerve fibers showed marked immunofluorescence.

Contol. Control staining without primary antibodies – or with specific blocking peptides of the primary antibodies – revealed no significant immunofluorescence (Figure 1).

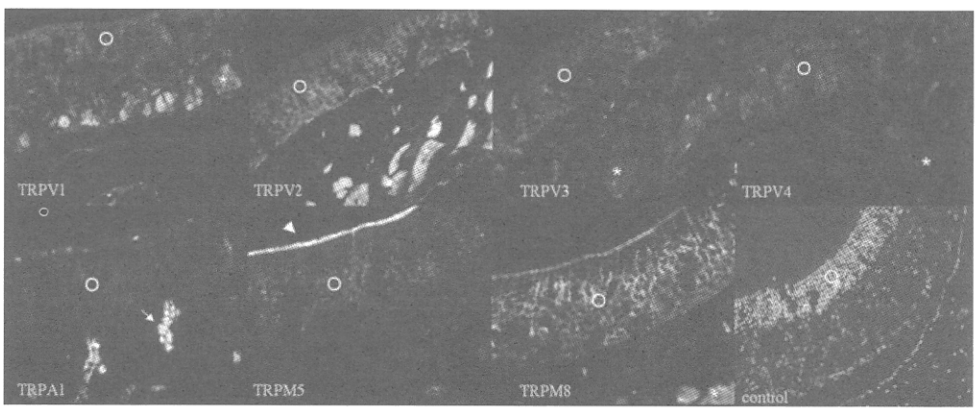

Figure 1. Immunofluorescent reaction to TRPV1 is evident in olfactory receptor neurons (ORNs). Supporting cells and basal cells are less intensely immunofluorescent. In lamina propria, nerve fibers (NFs) are immunofluorescent (TRPV1). Immunofluorescence to TRPV2 is evident in ORNs. Basal cells are markedly immunofluorescent. NFs are intensely immunofluorescent (TRPV2). Immunofluorescence to TRPV3 is observed in the ORNs. NFs show weak immunofluorescence (TRPV3). Immunofluorescence to TRPV4 is observed in the ORNs. In the lamina propria, TRPV4 labeling is weak and absent in NFs (TRPV4). The ORNs show immunofluorescence to TRPA1. Bowman's glands show marked immunofluorescence (TRPA1). Moderate immunofluorescence to TRPM5 is noted in the ORNs. Olfactory cilia are intensely immunofluorescent (TRPM5). Intense immunofluorescence to TRPM8 is observed in the ORNs. Olfactory cilia and basal cells are moderately immunofluorescent. NFs show marked immunofluorescence (TRPM8). Control staining without primary antibodies does not elicit immunofluorescence. Nuclei are counterstained with DAPI (control). O, ORNs; asterisk, nerve fiber; arrow, Bowman's gland; arrowhead, olfactory cilia.

Changes in expression of TRPs in methimazole-treated mouse OE

One day after treatment with methimazole, a thin, disorganized neuroepithelium was observed throughout the olfactory region. ORNs had almost completely disappeared, remaining only in a few basal cells. One week later, OE showed signs of recovery but was still thin and disorganized. One month after the treatment, OE had become thicker and had regained its normal appearance and thickness after 3 months.

In general, the immunoreactivity of ORNs to TRPV1 was markedly weaker 7 days after the methimazole treatment, although a few cells were immunofluorescent. The immunofluorescence of some ORNs had recovered after 1 month and showed complete recovery after 3 months. In the lamina propria, the nerve fibers were noticeably less immunofluorescent after 1 and 7 days and 1 month and showed normal fluorescence after 3 months. The immunoreactivity to TRPV2 was weaker in most ORNs, although a few cells showed intense fluorescence 7 days after the treatment. After 1 month, some cells were intensely fluorescent, while others still showed weaker fluorescence. After 3 months, the immunofluorescence of ORNs had returned to normal levels of intensity. In the lamina propria, the nerve fibers were markedly less immunofluorescent after 1 and 7 days and 1 month, but had regained normally strong fluorescence after 3 months. The immunoreactivity of ORNs to both TRPV3 and TRPV4 was weaker 7 days and 1 month after treatment, but after 3 months had returned to normal. The immunoreactivity of ORNs to TRPA1 was weaker after 7 days and 1 month, but had returned to normal after 3 months. The immunoreactivity of ORNs to TRPM5 was weaker after 7 days and 1 month but there was no fluorescence in the olfactory cilia, whereas after 3 months, fluorescence was normal in ORNs and intense in the olfactory cilia. The immunoreactivity to TRPM8 was slightly weaker, but still strong after 7 days and 1 month, and had recovered after 3 months (Figure 2).

Fluorescence intensity (normal mice)

TRPV1. Immunoreactivity in normal ORNs was 62 ± 2.0 (mean ± SD), decreasing significantly ($p < 0.01$) to 30 ± 10.6 after 7 days of treatment, had almost recovered (56 ± 14.0) after 1 month, and was normal again (68 ± 8.6) after 3 months. The difference in fluorescence intensity between 7 days and 1 month after treatment was significant ($p < 0.01$).

TRPV2. Immunoreactivity in normal ORNs was 80 ± 25.9, decreasing significantly ($p < 0.01$) to 31 ± 10.2 after 7 days, was 48 ± 15.1 after 1 month ($p < 0.01$), and had recovered to 83 ± 17.2 after 3 months. The difference in intensity between 7 days and 1 month after treatment was significant ($p < 0.05$).

TRPV3. Immunoreactivity in normal ORNs was 79 ± 20.1, had decreased significantly ($p < 0.01$) after 7 days, to 51 ± 4.3 after 1 month ($p < 0.01$), and had recovered to 87 ± 14.8 after 3 months.

TRPV4. Immunoreactivity in normal ORNs at 79 ± 24.5 had decreased significantly 7 days later ($p < 0.01$) and to 43 ± 9.7 after 7 days ($p < 0.01$) and was 40 ± 9.5 after 1 month ($p < 0.01$), but had recovered to 76 ± 21.3 after 3 months.

TRPA1. Immunoreactivity in normal ORNs was 59 ± 12.6, had decreased significantly ($p < 0.01$) to 29 ± 7.7 after 7 days, was 26 ± 8.2 ($p < 0.01$) after 1 month, and had recovered to 55 ± 13.7 after 3 months.

TRPM5. Immunoreactivity in normal ORNs at 66 ± 24.5 had decreased significantly ($p < 0.01$) to 26 ± 7.3 after 7 days and 27 ± 6.1 after 1 month. It had recovered to 55 ± 15.5 after 3 months.

TRPM8. Immunoreactivity in normal ORNs at 141 ± 33.2 was significantly weaker ($p < 0.01$) at 115 ± 31.8 after 7 days and 117 ± 40.6 after 1 month ($p < 0.1$) but had normalized to 138 ± 30.1 after 3 months (Figure 3).

Discussion

There is accumulating evidence that TRP channels are involved in thermosensation, mechanosensation, smell, and taste. From bacteria to man, food detection and acquisition are fundamental to survival. All the senses are required to make decisions about ingestion, and TRP channels, abundantly present in the nerve endings of the mouth, tongue, and nose, play an important role in chemical sensing [1,2]. In the OE, TRPC1 and 6, TRPM3, 4, 5, 6, and 7, TRPV2 and 6, and TRPA1 have been shown to be expressed by RT-PCR [4]. Expression of TRPV1, 2, 3, and 4, and TRPM5 has also been demonstrated by immunohistochemistry [3,6].

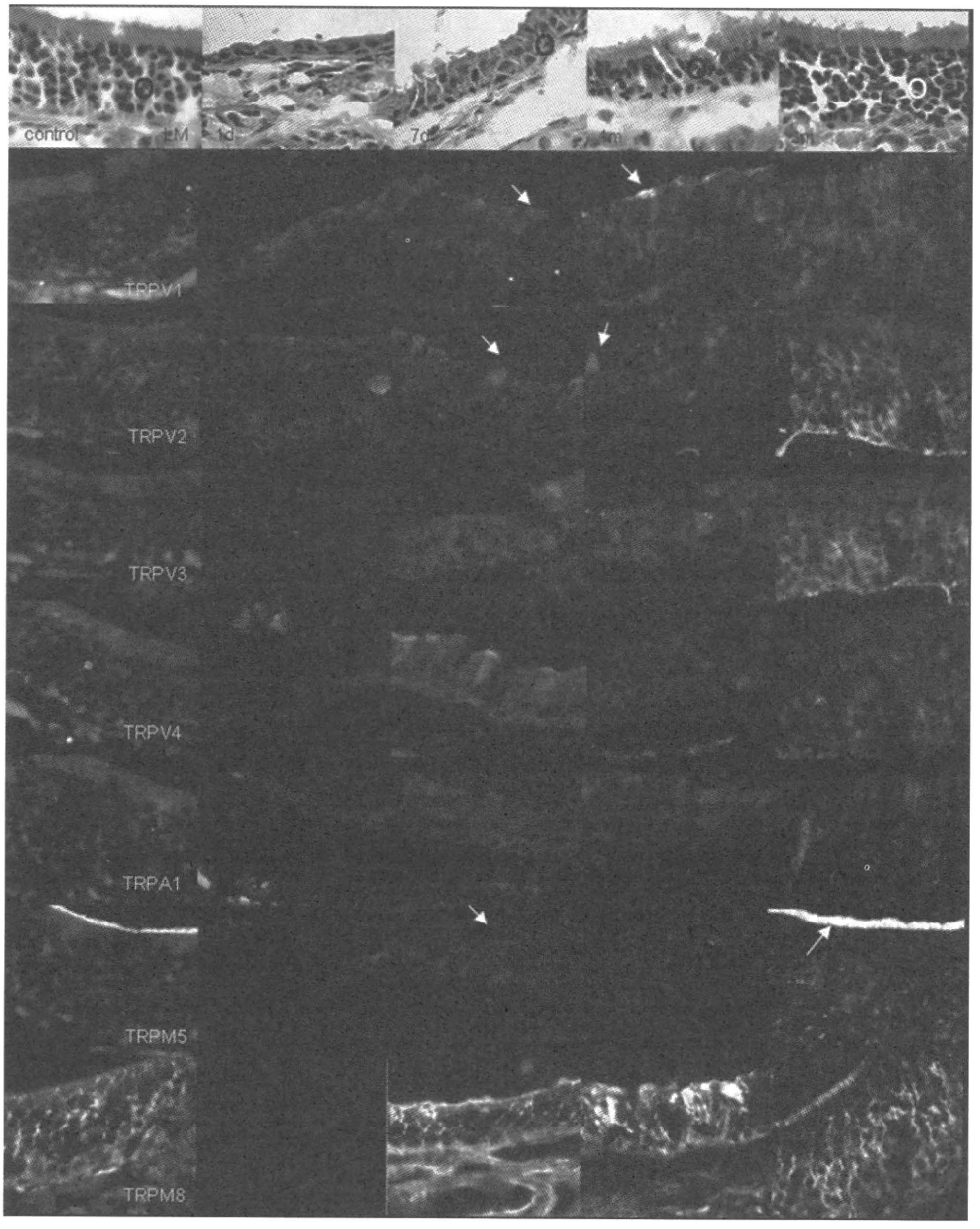

Figure 2. At 1 day after methimazole treatment (1d), there is a thin and disorganized neuroepithelium in the whole olfactory epithelium (OE; O). ORNs have almost completely disappeared. At 7 days later, OE shows signs of recovery but is still thin and disorganized (7d). At 1 month after treatment (1m), the OE is thicker, and after 3 months (3m) has regained its normal appearance and thickness. In general, the immunoreactivity of ORNs to TRPV1 is markedly reduced 7 days after methimazole treatment. A few cells show immunofluorescence (arrow). Immunofluorescence of ORNs has almost recovered (arrow) after 1 month and shows complete recovery after 3 months (TRPV1). Immunoreactivity of ORNs to TRPV2 is reduced in most ORNs, while a few cells show marked fluorescence (arrow) 7 days after the treatment. After 1 month, some cells show intense fluorescence (arrow), while others still show weaker fluorescence (TRPV2). Immunoreactivity of ORNs to TRPV3, TRPV4, and TRPA1 is reduced 7 days and 1 month after treatment. Immunoreactivity to TRPM5 is reduced after 7 days and 1 month. There is no fluorescence in olfactory cilia (arrow), while after 3 months, ORNs show normal fluorescence and there is intense staining in the olfactory cilia (arrow) (TRPM5). The immunoreactivity to TRPM8 is slightly weaker, but still strong after 7 days and 1 month, recovering to normal after 3 months (TRPM8).

The present study revealed immunoreactivity by TRPV1, 2, 3, and 4, TRPM5 and 8, and TRPA1 in murine OE, which confirms those previous investigations [3,4,6]. As regards the functional role of TRPVs, it has been suggested that TRPV1 may be involved in regulating cyclic nucleotide-gated channels and in short-term adaptation of the olfactory system [3]. Our finding of the presence of TRPV1 and TRPV2 in the ORNs, as well as in nerve fibers in the lamina propria, suggests that these TRP channels

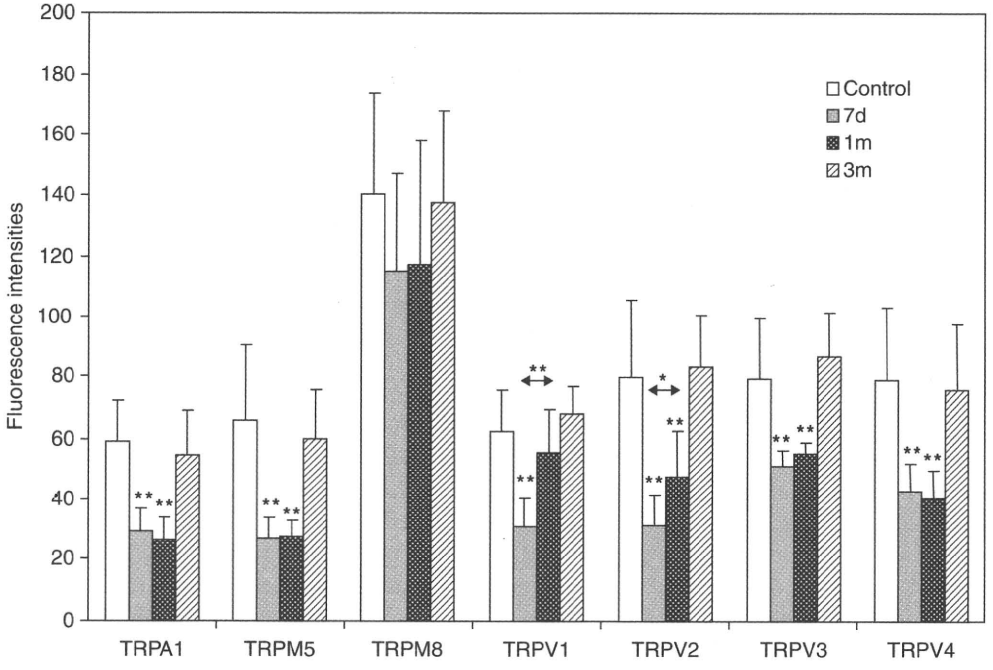

Figure 3. The fluorescence intensity to TRPV1 decreases significantly after 7 days but has normalized after 3 months. There is a significant difference in fluorescence intensity between 7 days and 1 month after. The intensity decreases significantly after 7 days and 1 month, with a significant difference between these two time points. The fluorescence intensities to TRPA1, TRPM5, TRPV3, and TRPV4 are significantly reduced after 1 month and 3 months, but have normalized after 3 months. The fluorescence intensity to TRPM8 is weaker but not significant after 7 days and 1 month. $^{**}p < 0.01$, $^{*}p < 0.05$.

play a vital part in chemosensation by OE. Furthermore, TRPV1 is known to be expressed in the nasal trigeminal neurons and showed sensitivity to capsaicin [7]. Taken together, all these findings indicate that TRPV1 and TRPV2 play an important role in the peripheral and central olfactory/trigeminal interaction in nasal chemoreception. TRPV3 may underlie the mechanism of enhanced oral and nasal sensitization to successive exposures to certain odors, flavors, and irritants [8]. Consequently, it has been suggested that TRPV3 acts as a chemoesthetic receptor and is also involved in allergic rhinitis caused by repeated exposures to certain odors. TRPV4 is activated by heat and extracellular hypotonicity. Hypotonicity-induced activation of TRPV4 requires its interaction with the water channel aquaporin (AQP) 5 [9]. It has been reported that the response of the frog's olfactory system to water is elicited by reduced osmotic pressure [10]. In addition, an extensive network of AQP, including AQP5 expression, is present in the OE [11]. These findings indicate that TRPV4 is directly involved in fluid homeostasis in the OE.

TRPA1 is the only TRPA protein present in humans and other mammals. TRPA1 is activated chemically by the psychoactive component in marijuana, by environmental irritants, and by pungent compounds. These include ingredients present in wasabi, horseradish, and mustard oils (isothiocyanates); garlic (allicin); cinnamon oil (cinnamaldehyde); marijuana (tetrahydrocannabinol); and tear gas (acrolein). TRPA1 can also be activated by stimulating the PLC pathway with bradykinin and the subsequently produced metabolites DAG and PUFAs [1,9].

It has not been conclusively established whether TRPA1 is a thermally or a mechanically gated channel. When exogenously expressed in cultured cells, TRPA1 has been reported to be a channel activated by injurious cold (< 17°C), although such activation in both cultured cells and TRPA1-deficient mice is controversial. TRPA1 channels in mouse and zebra fish have been suggested to be mechanically gated channels, and the multiple ankyrin repeats of TRPA1 may constitute a gating spring capable of transducing mechanical force and thereby facilitating channel opening. However, analyses of TRPA1-deficient mice have refuted this possibility [1,9].

The present investigation has demonstrated that immunoreactivity to TRPA1 occurred in the ORNs, while the nerve fibers in the lamina propria showed weak immunoreactivity. TRPA1 is reportedly present in neurons of dorsal root ganglia (DRG) and trigeminal ganglia (TG) [1,9]. TRPA1 immunoreactivity was found in unmyelinated nerve fibers in the urothelium, in the suburothelial space, and in the muscle layer, as well as around blood vessels

throughout the bladder [12]. All TRPA1 immunoreactive nerve fibers also expressed TRPV1 immunoreactivity and vice versa. TRPA1 was also detected in urothelial cells at both the transcriptional and the protein level. The presence of TRPA1 on C-fiber bladder afferents and in urothelial cells, and the finding that intravesical TRPA1 activators initiate detrusor hyperactivity, together indicate that TRPA1 participates in sensory transduction in this organ [12]. Our present findings mean that TRPA1 is also involved in chemosensation at the ORN level.

TRPM4 and TRPM5 are unusual in the TRP subfamily in that they are voltage-modulated, Ca^{2+}-activated, monovalent cation selective channels. The monovalent selectivity, which sets these channels apart from other TRP channels, is warranted by a short acidic sequence of six amino acids in its pore loop. TRPM5 is also temperature-sensitive, being activated by heat in the range of 15–35°C. It is thus another example of a TRP channel that integrates thermal input with other modes of activation [1,9]. TRPM5 protein has been demonstrated in intestine, liver, lung, and taste bud cells [1,9]. Recently, TRPM5 was shown to be enriched in taste receptor cells, where it is essential for the perception of sweet, bitter, and umami taste compounds. Two independently generated TRPM5 knockout mouse models display diminished sweet, bitter, and umami perception. Interestingly, the sensitivity of TRPM5 to temperature was suggested to be the molecular mechanism underlying the psychophysical phenomenon of 'thermal taste', i.e. enhanced sweetness perception with increasing temperature. TRPM5 is highly abundant in rodent chemosensory organs including OE and the vomeronasal organ (VNO), as well as in a subset of solitary cells distributed throughout the epithelia of the respiratory system and the gastrointestinal tract [13]. In the main OE, TRPM5 was detected in solitary epithelial cells. Occasionally, like typical ciliated olfactory cells, TRPM5-expressing cells have elongated cell bodies that reach both the lumen and the basal membrane. Furthermore, TRPM5 was detected in sensory epithelia of the VNO [13], in the apical part of the cell, and in the present study, also in the ORNs, especially on the apical surface. These data suggest that TRPM5 might play an as yet unappreciated physiological role in olfaction of odorants and pheromones.

TRPM8 is a thermally regulated channel activated by moderately cool temperatures (<23–28°C) and by agents that evoke a sensation of coolness, such as menthol, eucalyptol, and icilin. Activation by cold and menthol can be separated, as several mutations that have a profound effect on activation by menthol have only a minimal effect on activation by coolness. This shows that the domains involved in activation by menthol and thermal input are distinct. In further support of this conclusion, modulation of TRPM8 activity by pH has differential effects on activation by icilin and cold, versus menthol. The mechanisms for thermal activation of TRPV1 and TRPM8 by hot and cool temperatures, respectively, appear to be similar. These channels are voltage dependent, and their respective activation temperatures as well as ligands lead to shifts in their voltage thresholds toward more physiological membrane potentials [1,9]. TRPM8 protein has been demonstrated in DRG, TG, prostate, and liver [1,9]. The present study showed that TRPM8 was expressed mainly in the ORNs. These findings strongly indicate that TRPM8 is an essential factor in chemosensation in the OE and is probably related to the direct temperature reaction of the olfactory system to cool temperatures.

It has been demonstrated that at intermediate odorant concentrations, heat invariably causes a reduction in olfactory sensitivity, as they would be expected to compensate for the increase in volatiles in the air. Cold has the opposite effect [5]. These findings may indicate the existence of thermosensitive channels in the OE. Numerous mammalian TRP channels (thermo-TRPs), activated by temperature changes, account for a large proportion of the temperature range to which mammals respond. TRPV1 and TRPV2 are sensors for uncomfortably warm (>43°C) and very hot (>52°C) temperatures, respectively, whereas TRPV3 (>30–39°C) and TRPV4 (25–34°C) contribute to the perception of moderate temperatures. TRPM8 appears to function at cool temperatures, and TRPA1 may be a cold sensor [1]. Thermo-TRPs are present in neurons, such as those in the DRG or TG, which are known to function in thermosensation. Sensory neurons derived from TRPM8-null mice lack detectable levels of TRPM8 mRNA and protein and their number responding to cold (18°C) and menthol (100 μM) is greatly reduced [14]. These thermo-TRPs (TRPV1–4, TRPM8, and TRPA1) were all found in OE. The basis for previous and present findings is that these TRPs may function as thermosensitive calcium channels in the OE.

Several in vivo experimental models have been established for inducing mass degeneration of the ORNs. These include olfactory bulbectomy, olfactory nerve transection, topical application of chemicals such as zinc sulfate, Triton X-100, and methyl bromide into the nasal cavity, and systemic injection of nasotoxic drugs such as 3-methylindole, dichlobenil, and methimazole. The mode of cell death in the ORNs differs among these experimental models. Olfactory bulbectomy and olfactory nerve transection, which resemble olfactory dysfunction caused by head

injuries, have been found to induce massive apoptosis in the mature ORN population. In contrast, when applied to ORNs most chemicals that potentially resemble toxic environmental stimuli have been reported to cause necrosis. Regarding methimazole-induced cell death, chiefly in the mature ORNs, the affected cells were TUNEL-positive and showed a nuclear staining pattern, which strongly suggests that such cell death in ORNs is predominantly due to apoptosis [15].

The present study revealed that the fluorescence intensity of TRPs of murine ORNs was weakened by methimazole treatment. These effects were sustained until 3 months after the treatment, indicating that the recovery of TRP expression takes a long time, which might explain the clinical condition that recovery of the sense of smell, lost due to head injury, is also a lengthy procedure. The other interesting results were that expression of TRPM8 was not reduced following methimazole treatment. Moreover, expression of TRPV1 and TRPV2 recovered earlier. In the clinical situation of patients with olfactory disturbance, menthol and curry odors are frequently identified, but Japanese orange, wood, and condensed milk odors, seldom, since menthol odorants stimulate not only the olfactory nervous system but also the trigeminal nerve system [13]. As has been noted, TRPM8 is a thermally regulated channel activated by moderately cool temperatures (<23–28°C) and by compounds that evoke a sensation of coolness, such as menthol, eucalyptol, and icilin. TRPV1 is activated by capsaicin and resiniferatoxin, heat, H^+, and encocannabinoid [1,9]. Expression of both TRPV1 and TRPM8 was demonstrated in the TG [13]. It is plausible that menthol and/or curry odors stimulate the trigeminal nerve system, although the present study found unreduced expression of TRPM8 or early recovery of TRPV1 in the ORNs. These findings may indicate another possibility – that unchanged or early recovery of TRPV1 and TRPM8 in the ORNs is closely related to the fact that patients with olfactory disturbance display a high rate of recognition of menthol and curry odors. The early recovery of TRPV2 is another interesting finding. It has been suggested that TRPV2 is important in the regeneration of ORNs by stimulating nerve growth factors [17]. The early recovery of TRPV2 expression observed in our study seems to support this hypothesis.

In conclusion, our study has identified TRPV1, 2, 3, and 4, TRPM5 and 8, and TRPA1 in the mouse OE, where their presence seems to play a vital role, contributing to olfactory chemosensation, olfactory adaptation, olfactory/trigeminal interaction, and OE fluid homeostasis. In the pathological condition, the expression of TRPV3, TRPV4, TRPM5, and TRPA1 was markedly reduced and recovery took a long time. In contrast, expression of TRPM8 was only minimally affected even in the pathological condition, while TRPV1 and TRPV2 showed early recovery after methimazole treatment.

Acknowledgment

We thank Ms Ai Kashima for excellent technical assistance.

Declaration of interest: The authors report no conflicts of interest. The authors alone are responsible for the content and writing of the paper.

References

[1] Nilium B, Owsianik G, Voets T, Peters JA. Transient receptor potential cation channels in disease. Physiol Rev 2007;87: 165–217.

[2] Talavera K, Nilius B, Voets T. Neuronal TRP channels: thermometers, pathfinders and life-savers. Trends Neurosci 2008;31:287–95.

[3] Khalifa M, Takumida M, Ishibashi T, Hamamoto T, Hirakawa K. Expression of transient receptor potential vanilloid (TRPV) families 1, 2, 3 and 4 in the mouse olfactory epithelium. Rhinology 2009;47:242–7.

[4] Kamiyama N, Matsui H, Kashiwayanagi M. TRP channels expressing in murine olfactory epithelium. Japanese Taste and Smell 2006;13:559–60.

[5] Riveron J, Boto T, Alcorta E. The effect of environmental temperature on olfactory perception in Drosophila melanogaster. J Insect Physiol 2009;55:943–51.

[6] Lin W, Margolskee R, Donnert G, Hell SW, Restrepo D. Olfactory neurons expressing transient receptor potential channel M5 (TRPM5) are involved in sensing semichemicals. Proc Natl Acad Sci U S A 2007;104:2471–6.

[7] Damann N, Rothermel M, Klupp BG, Mettenleiter TC, Hatt H, Wetzel CH. Chemosensory properties of murine nasal and cutaneous trigeminal neurons identified by viral tracing. BMC Neurosci 2006;7:46.

[8] Xiao R, Tang J, Wang C, Calton CK, Tian J, Zhu MX. Calcium plays a central role in sensitization of TRPV3 channel to repetitive stimulations. J Biol Chem 2008;283: 6162–74.

[9] Venkatachalam K, Montell C. TRP channels. Annu Rev Biochem 2007;76:387–417.

[10] Sugawara M, Kashwayanagi M, Kurihara K. Water response of frog olfactory system is induced by a decrease in osmotic pressure. Brain Res 1990;510:326–8.

[11] Ablimit A, Matsuzaki T, Tajika Y, Aoki T, Hagiwara H, Takata K. Immunolocalization of water channel aquaporins in the nasal olfactory mucosa. Arch Histol Cytol 2006;69: 1–12.

[12] Streng T, Axelsson HE, Hedlund P, Andersson DA, Jordt S-E, Bevan S, et al. Distribution and function of the hydrogen sulfide-sensitive TRPA1 ion channel in rat urinary bladder. Eur Urol 2008;53:391–9.

[13] Laska M, Distel H, Hudson R. Trigeminal perception of odorant quality in congenitally anosmic subjects. Chem Senses 1997;22:447–56.

[14] Colbum RW, Lubin ML, Stone DJ Jr, Wang Y, Lawrence D, D'Andrea MR, et al. Attenuated cold sensitivity in TRPM8 null mice. Neuron 2007;54:379–86.

[15] Sakamoto T, Kondo K, Kashio A, Suzukawa K, Yamasoba T. Methimazole-induced cell death in rat olfactory receptor neurons occurs via apoptosis triggered through mitochondrial cytochrome c-mediated caspase-3 activation pathway. J Neurosci Res 2007;86:548–57.

[16] Kobayashi M, Nishida K, Nakamura S, Oishi M, Shinozaki T, Majima Y, et al. Stability of the odor stick identification test for the Japanese in patients suffering from olfactory disturbance. Acta Otolaryngol Suppl 2004;553: 74–9.

[17] Kamiyama N, Matsui H, Takakusaki K, Kashiwayanagi M. Physiological roles of TRPV2 expressed in the olfactory axon. Japanese Taste and Smell 2007;14:489–42.

Acta Oto-Laryngologica, 2008; 128: 22–28

informa
healthcare

CASE REPORT

Changes in slow phase eye velocity and time constant of positional nystagmus at transform from cupulolithiasis to canalolithiasis

TAKAO IMAI[1,2], NORIAKI TAKEDA[3], GO SATO[3], KAZUNORI SEKINE[3], MAHITO ITO[2], KOJI NAKAMAE[4] & TAKESHI KUBO[1]

[1]*Department of Otolaryngology, Osaka University Medical School, Osaka,* [2]*Department of Otolaryngology, Kansai-Rosai Hospital, Hyogo,* [3]*Department of Otolaryngology, University of Tokushima School of Medicine, Tokushima and* [4]*Department of Information Systems Engineering, Osaka University Graduate School of Engineering, Osaka, Japan*

Abstract

Changes in slow phase eye velocity (SPEV) and time constant (TC) of benign paroxysmal positional nystagmus in horizontal canal type were examined at transitional period from cupulolithiasis (apogeotropic nystagmus) into canalolithiasis (geotropic nystagmus) in two patients. SPEV and TC of positional nystagmus were tri-dimensionally analyzed. The first patient showed an apogeotropic nystagmus. Head rotation to the left in supine position induced a right-beating nystagmus with an initial SPEV of 15.3°/s and a TC of 133 s. The nystagmus then gradually declined with a TC of 31.3 s after reaching a maximum SPEV of 28.8°/s. After the nystagmus disappeared, he showed a geotropic nystagmus. The second patient showed a left-beating nystagmus with an initial SPEV of 2.5°/s and a TC of 141 s when his head was rotated to the right in supine position. The nystagmus then gradually declined with a TC of 8.05 s after reaching a maximum SPEV of 16.7°/s. After the nystagmus disappeared, he showed a geotropic nystagmus. The present findings suggested that in both patients, at the period of an increase of SPEV of the positional nystagmus with the shortening of its TC, cupulolithiasis transformed into canalolithiasis.

Keywords: *benign paroxysmal positional vertigo, apogeotropic nystagmus, geotropic nystagmus, rotation vectors, three-dimensional eye positions*

Introduction

Cupulolithiasis [1] in the horizontal semicircular canal (HSCC) has been shown to cause an apogeotropic positional nystagmus [2], while canalolithiasis in the HSCC causes a geotropic positional nystagmus [3] in patients with the HSCC type of benign paroxysmal positional vertigo (H-BPPV) [2,4]. Transition from a geotropic positional nystagmus to an apogeotropic positional nystagmus in the same patients with H-BPPV has been reported [5], suggesting the transformation from canalolithiasis into cupulolithiasis in HSCC. In the present study, we report two cases with transition from an apogeotropic positional nystagmus to a geotropic positional nystagmus. After analyzing their positional nystagmus in three dimensions, changes in slow phase eye velocity (SPEV) and time constant (TC) were examined at transitional period from cupulolithiasis to canalolithiasis in HSCC.

Case reports

Case 1

On May 18, 2001, an 80-year-old man visited our hospital complaining of a 2-day history of positional vertigo when turning over in bed. Based on his positional nystagmus, he was given the diagnosis of H-BPPV. His positional vertigo gradually disappeared without any canalith repositioning maneuver and on June 12, no positional nystagmus was noticed. He had no canal paresis in the caloric test, with no other neurological signs. Past medical history was notable for sudden sensorineural hearing loss of the left ear in 1948.

Correspondence: Takao Imai, MD, PhD, Department of Otolaryngology, Osaka Seamen's Insurance Hospital, 1-8-30 Chikkou, Minato-ku, Osaka-shi, Osaka 552-0021, Japan. Tel: +81 6 6572 5721. Fax: +81 6 6573 2531. E-mail: imaitakao@hotmail.com

(Received 11 January 2007; accepted 15 February 2007)

ISSN 0001-6489 print/ISSN 1651-2551 online
DOI: 10.1080/00016480701283752

Case 2

On February 27, 2006, a 46-year-old man visited our hospital with a complaint of positional vertigo from the same day when turning over in bed. He had been admitted to our hospital to undergo chemotherapy for his lung cancer, and based on his positional nystagmus, was given the diagnosis of H-BPPV. His positional vertigo gradually disappeared without any canalith repositioning maneuver. On April 14, he showed no positional nystagmus. He had no canal paresis in the caloric test and no hearing loss, with no other neurological signs.

Methods

Positional nystagmus of the left eye was recorded on videotape with an infrared CCD camera (RealEyes, Micromedical Technologies). In this paper, the tridimensional eye movements were described by rotation vectors, which represent the three-dimensional eye positions by a single rotation. The rotation vector was given by the axis of rotation, and its length was proportional to the size of the rotation [6]. An eye position can be reached by rotating the eye from a reference position on a single axis. This eye position was represented by a vector along a single axis of which length was proportional to the angle of the rotation. The reference position was defined to be that assumed by the eye when the subject was looking straight ahead with the head kept upright, while straight ahead was defined as looking at a target which was located horizontally in front of the eye [6]. The analysis method of the eye rotation vectors and the accuracy of this method have already been described elsewhere [7,8]. We converted these videotape images into 30 Hz digital ones (640*480 dot) (PCV-R63K, SONY), from which we reconstructed the space coordinates of the center of the pupil and an iris freckle. These coordinates (X, Y, and Z) were defined so that the X-axis was parallel to

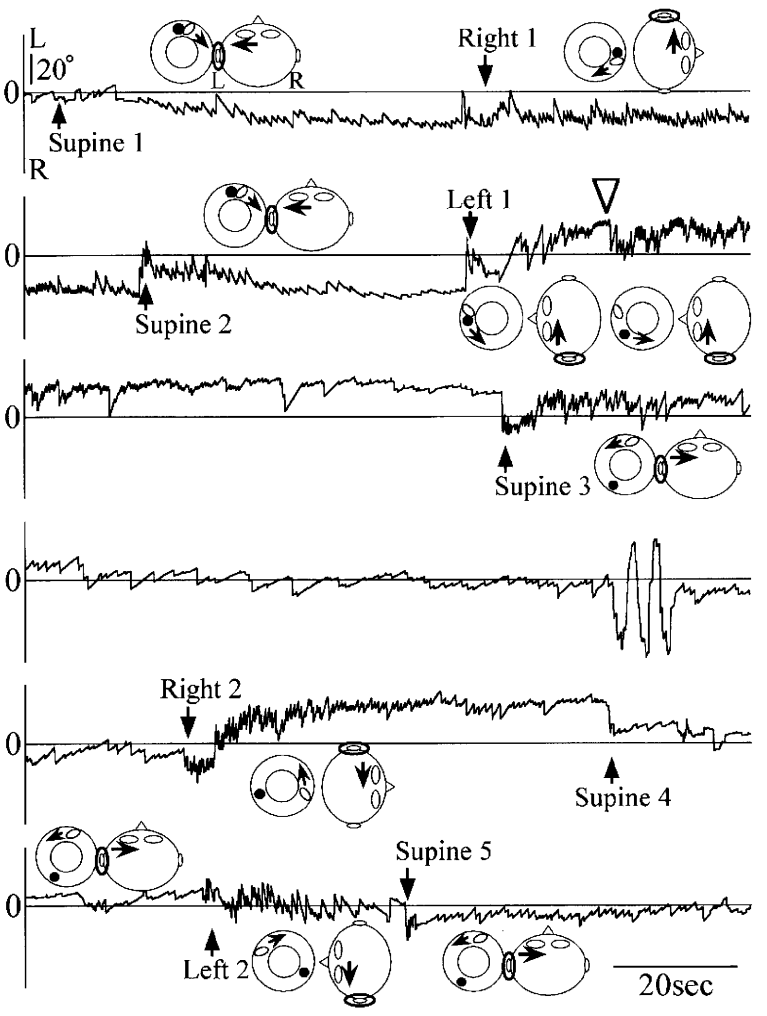

Figure 1. Eye position in Z component of positional nystagmus in patient 1. Inserted figures show his head position and his left HSCC with otocanial debris (●). The direction of the arrow near the eye of the inserted head figures shows the direction of his positional nystagmus. The direction of the arrow in the inserted HSCC figures shows the direction of deflection of the cupula.

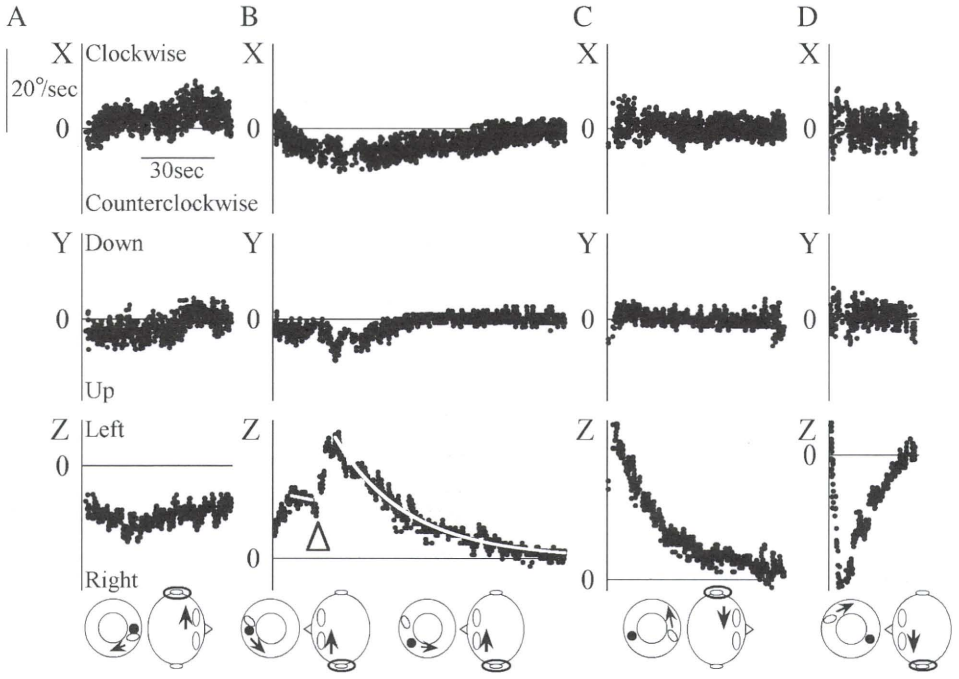

Figure 2. SPEV in X, Y, and Z components of positional nystagmus in patient 1 after his head was rotated to the right in supine position (Right 1 in Figure 1) (A), to the left (Left 1 in Fig. 1) (B), to the right again (Right 2 in Fig. 1) (C), and to the left again (Left 2 in Figure 1) (D). The SPEV and TC in Z component of positional nystagmus changed at the open triangle (V). The details of inserted figures are explained in the legend for Figure 1.

the naso-occipital axis (positive forward), Y-axis parallel to the inter-aural axis (positive left), and Z-axis normal to the X–Y plane (positive upwards). X, Y, and Z components mainly reflect the roll, pitch, and yaw components, respectively. The rotation vector $\mathbf{r}$ describing a rotation of θ about the axis $\mathbf{n}$ is given by the formula $\mathbf{r} = \tan(\theta/2) \times \mathbf{n}$, where $\mathbf{n}$ is a unit vector of which direction represents that of the axis. Because Euler angle is familiar, we used this parameter given as $2 \times \tan^{-1}$(magnitude of rotation vector) to represent the eye position as axis-angle representations [9]. The rotation vector of the eye position was $\mathbf{r}$, and using the following formula, $\boldsymbol{\omega} = 2 \times (d\mathbf{r}/dt + \mathbf{r} \times d\mathbf{r}/dt)/(1 + \mathbf{r}^2)$, we calculated the eye velocity $\boldsymbol{\omega}$ around X-, Y-, and Z-axes [6]. We extracted the slow phase data from nystagmic eye movement data by using the method [10–12].

Table. Maximum SPEV and TC of patients 1 and 2.

	Patient 1		Patient 2	
Parameter	Before the period shown by V	After the period shown by V	Before the period shown by V	After the period shown by V
Maximum SPEV	15.3°/s	28.8°/s	2.5°/s	16.7°/s
TC	133 s	31.3 s	141 s	8.05 s

Results

Case 1

Patient 1 showed a positional nystagmus mainly consisting of Z component, as shown in Figure 1. He showed a persistent left-beating nystagmus in the first supine position (Supine 1 in Figure 1), and when his head was firstly rotated to the right in supine position, he still showed a persistent left-beating nystagmus (Right 1 in Figure 1). After his head was returned to the straight-forward position in the second supine position, the left-beating nystagmus persisted (Supine 2 in Figure 1). The first rotation of the head to the left in supine position then induced a right-beating nystagmus, indicating apogeotropic positional nystagmus (Left 1 in Figure 1). After the right-beating nystagmus gradually disappeared, he showed a right-beating nystagmus in the third supine position (Supine 3 in Figure 1). Thereafter, patient 1 showed geotropic positional nystagmus as follows. When the head was rotated to the right again in supine, he showed a transient right-beating nystagmus (Right 2 in Figure 1). Subsequently, the second head rotation to the left in supine position induced a transient left-beating nystagmus (Left 2 in Figure 1). Finally, returning the head to the straight-forward in the fifth supine position triggered a right-beating nystagmus (Supine 5 in Figure 1).

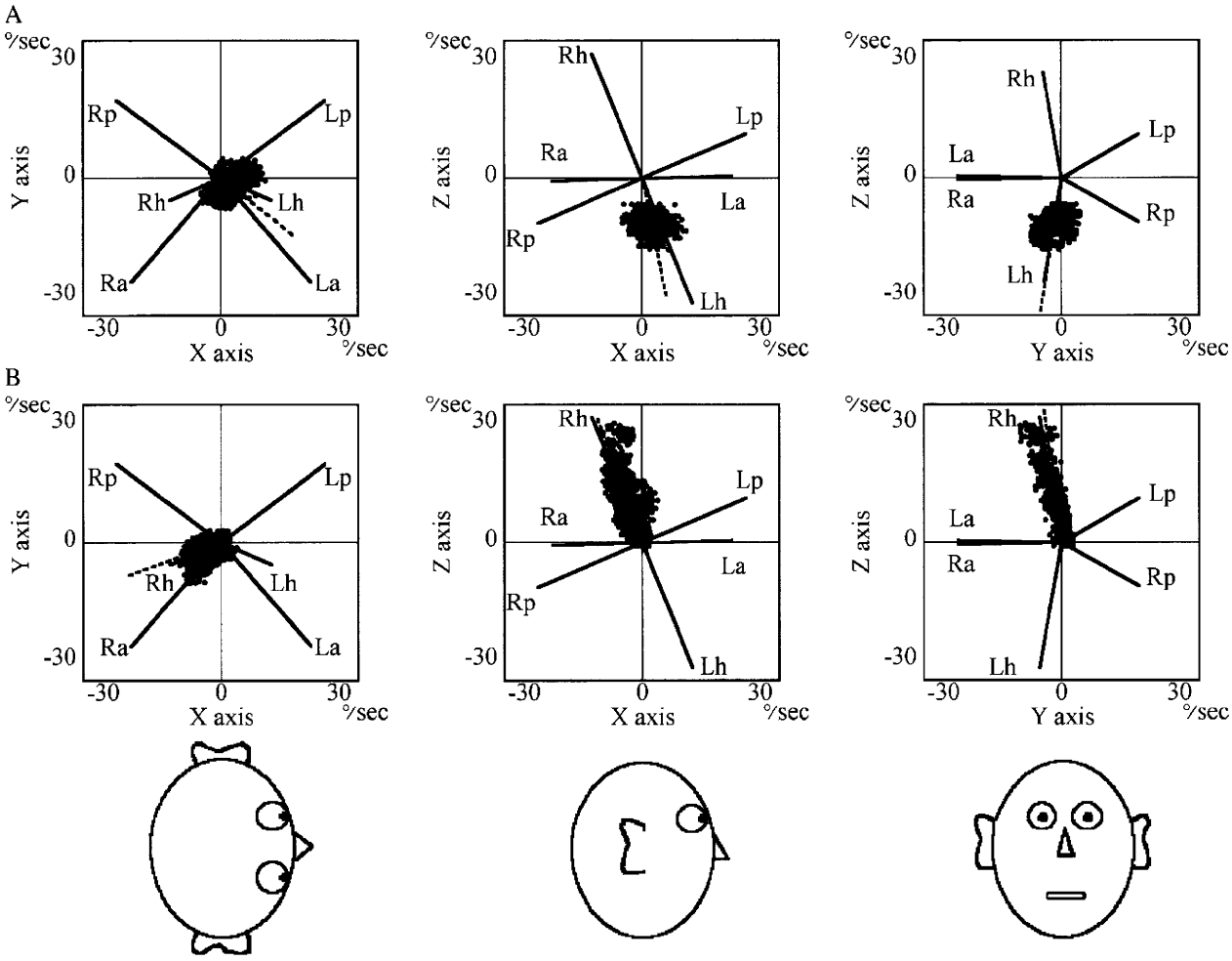

Figure 3. The rotation vectors of SPEV of the left-beating positional nystamus (Right 1 in Figure 1) (A) and those of the right-beating positional nystagmus (Left 1 in Figure 1) (B) in patient 1. Dotted line, the averaged rotation axis of SPEV; Ra, axis perpendicular to the plane of the right anterior semicircular canal; Rh, axis perpendicular to the plane of the right HSCC; Rp, axis perpendicular to the plane of the right posterior semicircular canal; La, axis perpendicular to the plane of the left anterior semicircular canal; Lh, axis perpendicular to the plane of the left HSCC; Lp, axis perpendicular to the plane of the left posterior semicircular canal [13].

SPEV of positional nystagmus in patient 1 is shown in Figure 2. In Figure 2A, the first rotation of the head to the right in supine position (Right 1 in Figure 1) induced a left-beating positional nystagmus mainly consisting of Z component that lasted for more than 60 s. In Figure 2B, when the head was conversely rotated to the left in supine position (Left 1 in Figure 1), a right-beating nystagmus at first lasted for 20 s with an initial SPEV of 15.3°/s and a TC of 133 s in Z component (Table). Then, SPEV in Z component suddenly increased at the period indicated by an open triangle symbol and gradually declined with a TC of 31.3 s after reaching a maximum SPEV of 28.8°/s (Figure 2B, Table). Using the least squares method, changes in Z component with time (t) were approximated by the formula: $15.3\exp(-(t-203)/133)$ for an initial 20 s period, and was approximated by $28.8\exp(-(t-220)/31.3)$ thereafter (gray line in Figure 2B).

In Figure 2C, when the head was rotated to the right again in supine position (Right 2 in Figure 1), SPEV in Z component of the right-beating nystagmus gradually declined. The second rotation of the head to the left in supine (Left 2 in Figure 1) also induced a gradual decline of SPEV in Z component of the left-beating nystagmus (Figure 2D).

The SPEV rotation vectors of positional nystagmus in Figure 2A and B are plotted on XY, XZ, and YZ planes in Figure 3. It was demonstrated that: (i) the axis of the persistent left-beating positional nystagmus in Figure 2A was perpendicular to the plane of the left HSCC (Lh) [13] in Figure 3A, and (ii) that the axis of the right-beating positional nystagmus in Figure 2B was perpendicular to the plane of the right HSCC (Rh) [13] in Figure 3B and its direction remained unchanged despite changes in SPEV and TC at the period indicated by an open triangle symbol in Figure 2B.

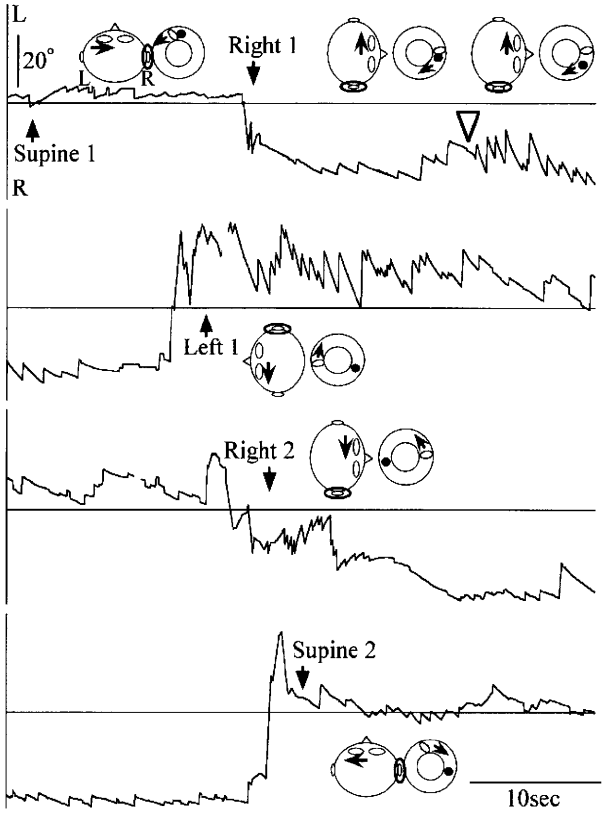

Figure 4. Eye position in Z component of positional nystagmus in patient 2. Inserted figures show his head position and his right HSCC with otocanial debris (●). The direction of the arrow near the eye of the inserted head figures shows the direction of his positional nystagmus. The direction of the arrow in the inserted HSCC figures shows the direction of deflection of the cupula.

Case 2

Patient 2 showed a positional nystagmus mainly consisting of Z component as shown in Figure 4. He showed a right-beating persistent nystagmus in the first supine position (Supine 1 in Figure 4). The first rotation of the head to the right in supine induced a persistent left-beating nystagmus for the initial 15 s that then gradually declined (Right 1 in Figure 4). Thereafter, patient 2 showed geotropic positional nystagmus as follows. When his head was firstly rotated to the left in supine position, he showed a transient left-beating nystagmus (Left 1 in Figure 4). When the head was rotated to the right again in supine position, he showed a transient right-beating nystagmus (Right 2 in Figure 4). When the head was returned to the straight-forward position in the second supine position, he showed a transient left-beating nystagmus (Supine 2 in Figure 4).

SPEV of positional nystagmus in patient 2 is shown in Figure 5. As shown in Figure 5A, the first rotation of the head to the right in supine (Right 1 in Figure 4) induced a left-beating nystagmus at first that lasted for a 15 s period with an initial SPEV of 2.5°/s and a TC of 141 s in Z component (Table). SPEV in Z component then suddenly increased at the period indicated by an open triangle symbol and gradually declined with a TC of 8.05 s after reaching a maximum SPEV of 16.7°/s (Figure 5A, Table). Using the least squares method, changes in Z component against time (t) were approximated by the formula: $-2.50\exp(-(t-74.6)/141)$ for the initial 15 s period and was approximated by $-16.7\exp(-(t-88.3)/8.05)$ thereafter (gray line in Figure 5A).

In Figure 5B, when the head was firstly rotated to the left in supine position (Left 1 in Figure 4), SPEV in Z component of the left-beating nystagmus gradually declined. In Figure 5C, when his head was rotated to the right again in supine (Right 2 in Figure 4), SPEV in Z component of the right-beating nystagmus also gradually declined.

Discussion

Patient 1 initially showed a persistent left-beating nystagmus in the right head-turning position and a right-beating nystagmus in the left head-turning position in supine (Figures 1 and 2A, and 2B). Based on his characteristic apogeotropic positional nystagmus, patient 1 was given the diagnosis of H-BPPV, suggesting the presence of cupulolithiasis in his HSCC. Although it is still controversial to determine the affected ear in patients with cupulolithiasis-induced apogeotropic positional nystagmus, our observation is in line with that of Bisdorff and Debatisse, who reported that the direction of nystagmus in supine position points to the affected ear in patients with cupulolithiasis [14]. Accordingly, we assumed that the HSCC of the left ear was affected by cupulolithiasis in patient 1.

The positional nystagmus in patient 1 then changed to a transient geotropic positional nystagmus (Figures 1 and 2C, and 2D), suggesting the presence of canalolithiasis in his HSCC. Therefore, it is suggested that in patient 1, cupulolithiasis transformed into canalolithiasis in the HSCC of the left ear.

It has been reported that the TC of apogeotropic positional nystagmus was longer compared with geotropic positional nystagmus in patients with H-BPPV [5,15,16]. Therefore, it is suggested that the TC of positional nystagmus induced by cupulolithiasis is prolonged, in comparison with that induced by canalolithiasis [17]. On the contrary, based on mathematical models, it was reported that SPEV of positional nystagmus induced by canalolithiasis is larger than that induced by cupulolithiasis [18,19]. In patient 1, SPEV of right-beating positional nystagmus suddenly increased

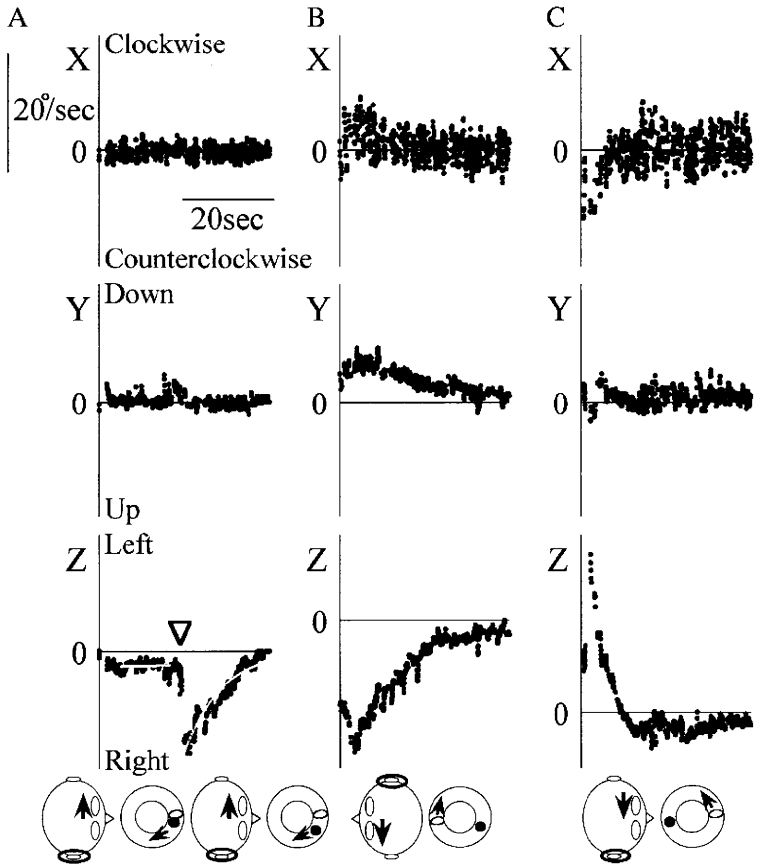

Figure 5. SPEV in X, Y, and Z components of positional nystagmus in patient 2 after his head was rotated to the right in supine position (Right 1 in Figure 4) (A), to the left (Left 1 in Figure 4) (B), and to the right again (Right 2 in Figure 4) (C). The SPEV and TC in the Z component of positional nystagmus changed at the open triangle (∇). The details of inserted figures are explained in the legend for Figure 4.

with the shortening of its TC by 20 s after the head was rotated to the left in supine position (Figure 2B, Table). Moreover, during changes in SPEV and TC, the axis of right-beating positional nystagmus remained perpendicular to the plane of the right HSCC (Figure 3B). Thereafter, he showed a transient geotropic positional nystagmus (Figure 2C and 2D). Therefore, the increase of SPEV of positional nystagmus with the shortening of its TC at transient period from an apogeotropic positional nystagmus into a geotropic positional nystagmus supports the hypothesis that the otoconial debris attached to the cupula that was deviated in the ampulofugal direction was released as free-floating debris in the left HSCC at this period. In the left head-turning position where the affected HSCC of the left ear is placed undermost, otoconia hanging inferiorly from the cupula may naturally fall through the canal in the ampulofugal direction by the gravity. Accordingly, the ampulofugal deflection of the cupula induced by both cupulolithiasis and canalolithiasis in the left HSCC may keep the axis of the right-beating positional nystagmus in the left head-turning position, which is perpendicular to the plane of the right HSCC during changes in SPEV and TC.

Fetter et al. showed that cold caloric stimulation of one ear induced nystagmus beating to the other ear, of which the axis is perpendicular to the plane of the HSCC of the other ear [20]. This is why in the transient period from cupulolithiasis into canalolithiasis in patient 1, the ampulofugal deflection of the cupula of the left HSCC produced by both cupulolithiasis and canalolithiasis remained to induce right-beating nystagmus, of which the axis is perpendicular to the plane of the right HSCC.

Based on the persistent right-beating nystagmus in supine position and the initial left-beating nystagmus in the head-right turning position (Figure 4), patient 2 was given the diagnosis of H-BPPV due to cupulolithiasis in the HSCC of the right ear [14], although positional nystagmus was not recorded in the left head-turning position in the patient. After his head was rotated to the right, SPEV of a right-beating positional nystagmus suddenly increased with the shortening of its TC (Figure 5A, Table), followed by the appearance of a transient geotropic positional nystagmus (Figure 5B, C). Therefore, it is

suggested that cupulolithiasis transformed into canalolithiasis by releasing otoconial debris from the cupula in the right HSCC in patient 2.

In the present study, we report changes in the SPEV and TC of positional nystagmus at the transitional period from cupulolithiasis into canalolithiasis in two patients with H-BPPV. Although our hypothesis is based on a limited number of subjects, an increase of SPEV of positional nystagmus with the shortening of its TC might be a clinical indicator of transition from an apogeotropic positional nystagmus into a geotropic one in patients with H-BPPV.

References

[1] Schuknecht HF. Cupulolithiasis. Arch Otorhinolaryngol 1969;90:765–78.
[2] Casani A, Giovanni V, Bruno F, Luigi GP. Positional vertigo and ageotropic bi-directional nystagmus. Laryngoscope 1997;107:807–13.
[3] Hall SF, Ruby RR, MaClure JA. The mechanics of benign paroxysmal vertigo. J Otolaryngol 1979;8:151–8.
[4] McClure JA. Horizontal canal BPV. J Otolaryngol 1985;14: 30–5.
[5] Steddin S, Ing D, Brandt T. Horizontal canal benign paroxysmal positioning vertigo (h-BPPV): transition of canalolithiasis to cupulolithiasis. Ann Neurol 1996;40:918–22.
[6] Haslwanter T. Mathematics of three-dimensional eye rotations. Vision Res 1995;35:1727–39.
[7] Imai T, Takeda N, Morita M, Koizuka I, Kubo T, Miura K, et al. Rotation vector analysis of eye movement in three dimensions with an infrared CCD camera. Acta Otolaryngol (Stockh) 1999;119:24–8.
[8] Imai T, Sekine K, Hattori K, Takeda N, Koizuka I, Nakamae K, et al. Comparing the accuracy of video-oculography and the scleral search coil system in human eye movement analysis. Auris Nasus Larynx 2005;32:3–9.
[9] Raphan T. Modeling control of eye orientation in three dimensions. I. Role of muscle pulleys in determining saccadic trajectory. J Neurophysiol 1998;79:2653–67.
[10] Arzi M, Mignin M. A fuzzy set theoretical approach to automatic analysis of nystagmic eye movements. IEEE Trans Biomed Eng 1989;36:954–63.
[11] Imai T, Takeda N, Ito M, Nakamae K, Sakae H, Fujioka H, et al. Three-dimensional analysis of benign paroxysmal positional nystagmus in a patient with anterior semicircular canal variant. Otol Neurotol 2006;27:362–6.
[12] Imai T, Takeda N, Ito M, Kakamae K, Sakae H, Fujioka H, et al. Benign paroxysmal positional vertigo due to a simultaneous involvement of both horizontal and posterior semicircular canals. Audiol Neurotol 2006;11:198–205.
[13] Blanks RH, Curthoys IS, Markham CH. Planar relationships of the semicircular canals in man. Acta Otolaryngol (Stockh) 1975;80:185–96.
[14] Bisdorff AR, Debatisse D. Localizing signs in positional vertigo due to lateral canal cupulolithiasis. Neurology 2001; 57:1085–8.
[15] Baloh RW, Yue Q, Jacobson KM, Honrubia V. Persistent direction-changing positional nystagmus: another variant of benign positional nystagmus? Neurology 1995;45:1297–301.
[16] Brandt T. Benign paroxysmal positioning vertigo. In: Brandt T, editor. Vertigo: its multisensory syndromes, 2nd edn. London: Springer-Verlag; 1999. p. 251–83.
[17] Steddin S, Brandt T. Unilateral mimicking bilateral benign paroxysmal positioning vertigo. Arch Otolaryngol Head Neck Surg 1994;120:1339–41.
[18] Squires TM, Weidman MS, Hain TC, Stone HA. A mathematical model for top-shelf vertigo: the role of sedimenting otoconia in BPPV. J Biomech 2004;37:1137–46.
[19] Rajguru SM, Ifediba MA, Rabbitt RD. Biomechanics of horizontal canal benign paroxysmal positional vertigo. J Vestib Res 2005;15:203–14.
[20] Fetter M, Aw S, Haslwanter T, Heimberger J, Dichgans J. Three-dimensional eye movement analysis during caloric stimulation used to test vertical semicircular canal function. Am J Otol 1998;19:180–7.

Acta Oto-Laryngologica, 2009; 129: 45–51

informa
healthcare

ORIGINAL ARTICLE

Effects of hypergravity on histamine H1 receptor mRNA expression in hypothalamus and brainstem of rats: implications for development of motion sickness

GO SATO[1], ATSUHIKO UNO[3], ARATA HORII[3], HAYATO UMEHARA[2], YOSHIAKI KITAMURA[1], KAZUNORI SEKINE[1], KOICHI TAMURA[1], HIROYUKI FUKUI[2] & NORIAKI TAKEDA[1]

[1]*Department of Otolaryngology,* [2]*Department of Molecular Pharmacology, Institute of Health Biosciences, University of Tokushima Graduate School, Tokushima and* [3]*Department of Otolaryngology, Osaka University School of Medicine, Osaka, Japan*

Abstract

Conclusion: The study findings suggest that histamine was released from the axon terminals in the hypothalamus and brainstem and the released histamine activated post-synaptic H1 receptors there, resulting in the development of motion sickness. *Objectives:* We first examined which subtype of post-synaptic histaminergic receptor was responsible for the development of motion sickness. We then examined whether H1 receptors were up-regulated in various areas of the rat brain after 2 G hypergravity load, because the stimulation of H1 receptor was reported to up-regulate the level of H1 receptor protein expression through augmentation of H1 receptor mRNA expression. *Materials and methods:* For this purpose, we used an animal model of motion sickness, using pica (eating non-nutritive substances such as kaolin), as a behavioral index in rats. *Results:* After 2 G hypergravity load, rats ate a significant amount of kaolin, indicating that they suffered from motion sickness. The hypergravity-induced kaolin intake was suppressed by mepyramine, but not by terfinadine or zolantizine. This finding indicates that cerebral post-synaptic H1 but not H2 or peripheral H1 receptors play an important role in the development of motion sickness. The expression of H1 receptor mRNA was up-regulated in the hypothalamus and brainstem, but not in the cerebral cortex after 2 G hypergravity load in rats.

Keywords: *Motion sickness, histamine, H1 receptor, kaolin, mepyramine, terfenadine, zolantidine, hypothalamus, brainstem*

Introduction

Humans without vestibular function never suffer from motion sickness, indicating that the vestibular system is essential for the development of motion sickness [1]. H1 blockers are clinically effective in preventing motion sickness [2,3], indicating that the histaminergic neuron system is important in the development of motion sickness. To investigate the vestibulo-histaminergic interaction in the processes of motion sickness, we developed an animal model of motion sickness in rats [4]. Rats cannot vomit, but pica, the intake of non-nutritive substances such as kaolin (hydrated aluminum silicate), is an illness response behavior of rats, which is analogous to vomiting. In the previous study, we showed that motion-induced pica is an index of motion sickness in rats [5].

A 2 G hypergravity load induced kaolin intake in rats, indicating that they suffered from motion sickness [6]. The hypergravity and caloric vestibular stimulation increased the release of histamine from the rat hypothalamus, suggesting that the activation of histaminergic neuron system in the hypothalamus through the vestibulo-histaminergic interaction plays an important role in the development of motion sickness [6,7]. In the present study, to investigate the post-synaptic events after the vestibulo-histaminergic interaction, we first used the animal model and examined which subtype of post-synaptic

Correspondence: Go Sato MD, Department of Otolaryngology, Institute of Health Biosciences, University of Tokushima Graduate School, 3-18-15 Kuramoto, Tokushima 770-8503, Japan. Tel: +81 88 633 7169. Fax: +81 88 633 7170. E-mail: go-sato@clin.med.tokushima-u.ac.jp

(Received 9 January 2008; accepted 24 February 2008)

ISSN 0001-6489 print/ISSN 1651-2251 online
DOI: 10.1080/00016480802008173

histaminergic receptor was responsible for the development of motion sickness. The effects of pretreatment by mepyramine, an H1-blocker, by terfenadine, an H1-blocker that does not cross the blood–brain barrier (BBB) or by zolantidine, a BBB-penetrating H2-blocker, on hypergravity-induced pica were examined in rats.

Recently it was reported that the stimulation of H1 receptor up-regulates the level of H1 receptor protein expression through augmentation of H1 receptor mRNA expression in HeLa cells and rat nasal mucosa [8,9]. These findings led to the idea that the expression of H1 receptor mRNA is increased by 2 G hypergravity load in the brain area to which the histaminergic activation is transmitted in the processes of motion sickness. So, we then examined whether H1 receptors were up-regulated in various areas of the rat brain after 2 G hypergravity load.

Materials and methods

Animals, kaolin preparation, and hypergravity stimulation

All animal experiments were approved by the Animal Care Committee of the University of Tokushima School of Medicine. Male Wistar strain rats weighing 250 g were used. They were kept in individual standard home cages ($35 \times 25 \times 45$ cm) with free access to food, water, and kaolin in a room with a 12 h light/12 h dark cycle (light from 8:30 to 20:30). Their sensitivity to motion sickness was assessed before the experiment and only susceptible animals were used. Accordingly the animals that consumed <1.0 g of kaolin after a 2 h load of hypergravity were excluded from the study, because this experiment was designed to assess the effect of anti-motion sickness drugs.

Pharmaceutical grade kaolin (hydrated aluminum silicate, Ishizu Pharmaceutical Co., Japan) was mixed with 1% arabic gum (Ishizu Pharmaceutical Co.) in distilled water to form a thick paste, which was extruded through a syringe onto wire mesh trays and partially dried at room temperature. This mixture was then introduced into a column of the same shape as that for food, and again dried completely at room temperature. The kaolin, provided in containers, was placed in the cage. The kaolin container was removed, weighed to the nearest 0.1 g, refilled, and replaced at 18:00 each day. Spilt kaolin was collected, dried, and weighed to obtain the correct values for kaolin consumption.

Hypergravity was produced by an animal centrifuge device [6]. The swing arm on which the animal cage was suspended was mounted 50 cm from the axis of a turntable driven by a servo-controlled torque motor. The turntable was rotated at a constant rate, loading the animal in the centrifuge cage with the vector sum of the gravity linear acceleration and a rotation centrifugal linear acceleration vectors. An angular velocity of 336°/s (56 rpm) achieved a resultant linear acceleration of 2 G acting on the animal along its back to abdomen axis.

Effects of histamine receptor blockers on hypergravity-induced kaolin intake

Kaolin was placed in the cage for 3 days before the hypergravity load was applied to allow the animals to become adapted to its presence. Following this adaptation period, animals were exposed to 2 G hypergravity for 2 h on the next day. Seven days after the first hypergravity load, animals were divided into four groups according to the administered drugs: saline group (Sal, $n=6$), mepyramine group (Mep, $n=6$), terfenadine group (Ter, $n=5$), and zolantidine group (Zol, $n=8$). Mepyramine (Sigma Chemical Co., Japan) and zolantidine (Nakarai tesuku Co., Japan) were dissolved in saline, while terfenadine (Nakaraitesuku Co., Japan) was dissolved in saline containing 0.05% carboxymethylcellulose. All of the drugs were administered intraperitoneally at a dose of 10 mg/kg. The dose of 10 mg/kg was decided on the basis of our previous study where diphenhydramine, another H1-blocker, suppressed rotation-induced kaolin intake dose-dependently at an optimal dose of 10 mg/kg. Control animals were injected with the same volume of saline. Each drug or saline was administered 30 min before the second hypergravity load. Kaolin consumption on day 4 indicated the amount of kaolin consumed during 24 h after the first hypergravity load, whereas that on day 11 indicated the kaolin consumption during 24 h after the second load. Ratio of kaolin intake on day 11 and day 4 (day 11/day 4) was calculated and used as an index of the drug effect.

Effects of hypergravity on H1 receptor mRNA expression

Animals were exposed to 2 G hypergravity for 0, 2, 4, 6, or 12 h. Control animals were in the animal cage placed beside the centrifuge device for the same period but were not exposed to hypergravity. Each group was made up of six animals and a total of 60 animals were used.

Dissection of tissues and isolation of total RNA

Just after exposure to the hypergravity load, animals were sacrificed under an overdose anesthesia with pentobarbital. The hypothalamus, brainstem, and cerebral cortex were carefully dissected with a sharp

blade under microscopic guidance. The hypothalamus was dissected by cutting the brain at the level of optic chiasm and mammillary nucleus. From this block, only the ventral part of the thalamus was removed while the dorsal part was used as a cerebral cortex specimen after removal of the hippocampus and more ventral parts. The brainstem was dissected from the level of abducens nucleus to the solitary tract nucleus. Changes in H1R mRNA expression in the hypothalamus were investigated at the five time points (0, 2, 4, 6, and 12 h), whereas changes in the brainstem and the cerebral cortex were measured only after 4 h load of hypergravity.

Samples were frozen in RNAlater (Takara Biochemicals, Tokyo, Japan) and stored in a tube at −80°C until assayed. Total RNA was isolated using TRIzol reagent (Invitrogen Corp., Carlsbad, CA, USA) in accordance with the manufacturer's instructions. Samples were then homogenized using a Polytron (Model PT-K; Kinematica AG, Littau/Luzern, Switzerland) in 10 volumes of ice-cold TRIzol reagent until completely homogenized before the homogenates were mixed with chloroform and centrifuged at 15 000 rev/min for 15 min at 4°C. The aqueous phase containing RNA was transferred to a new tube and the RNA was precipitated by addition of isopropanol. Samples were incubated at room temperature for 5 min and centrifuged at 15 000 rev/min for 15 min at 4°C. The RNA pellet was washed with 70% ice-cold ethanol, air-dried, and then dissolved in 20 μl of diethlyrocarbonate-treated water. The purity and yield of total RNA were determined spectrophotometrically at 260 and 280 nm. The ratio of absorption (260:280 nm) of all preparations was 1.8–2.0.

Real-time quantitative reverse transcription polymerase chain reaction

RNA samples were reverse-transcribed to cDNA in a 47 μl reaction volume in the presence of first-strand buffer (375 mM KCl, 250 mM Tris-HCl, pH 8.3, at room temperature), 15 mM $MgCl_2$, 0.8 mM concentrations of each deoxyribonucleoside triphosphate (dNTP), 40 μM oligo (dT) primers, 0.004 units of RNase inhibitor, and 8 units of the reverse transcriptase. Samples were incubated at 37°C for 60 min before adding 2.35 μl of 2 N NaOH and then incubating again at 65 °C for 30 min. Subsequently, 14.3 μl of 1 M Tris-HCl, pH 8.0, were added and the samples were then heated at 95°C for 10 min and chilled to 4°C for 5 min. TaqMan primers and probe were designed using the Primer Express primer design software (Perkin Elmer Applied Biosystems, Foster City, CA, USA). The sequences of primers were as follows: sense primer, 5′-TAT GTG TCC GGG CTG CAC T-3′; antisense primer, 5′-CGC CAT GAT AAA ACC ACC CAA CTG-3′. The sequence of the probe was as follows: FAM-CCG AGA GCG GAA GGC AGC CA-TAMRA. To account for differences in starting material, rodent glyceraldehyde-3-phosphate dehydrogenase (GAPDH) primers and probe reagents from Applied Biosystems were used as recommended by the manufacturer. The transcripts were utilized for a 40 cycle, three-step polymerase chain reaction (PCR) using the GeneAmp5700 Sequence Detection System (Perkin Elmer Applied Biosystems) in 20 mM Tris, pH 8.4, 50 mM KCl, 3 mM $MgCl_2$, 200 μM dNTPs, 900 nM concentrations of each primer, and 0.25 units of platinum Taq. Amplicon size and reaction specificity were confirmed using agarose gel electrophoresis. The identity of the PCR products was verified by sequencing using a DNA thermocycler (4200L-1; Alolka, Tokyo, Japan).

The number of target copies in each sample was interpolated from its detection threshold (C_T) value using a purified PCR product standard curve included on each plate. Each PCR run included the four points of the standard curve (threefold serially diluted cDNA), a no-template control, the calibrator cDNA, and the unknown cDNAs. The measurements were calibrated using the calibrator included on each PCR plate. For the quantification of gene expression, we used GAPDH RNAs as the endogenous control. To determine whether the amplification products came exclusively from the RNA, a reverse transcriptase (RT)-negative reaction was run in which the enzyme was replaced by RNase-free water for each sample.

H1R mRNA in the hypothalamus was expressed as a percentage of that of the 0 h load. H1R mRNA in the brainstem and the cerebral cortex were evaluated after only 4 h load of hypergravity and expressed as a percentage of that of control animals that were in the animal cage placed beside the centrifuge device.

Effects of labyrinthectomy on hypergravity-induced H1 receptor mRNA expression

Under general anesthesia induced by sodium pentobarbital (50 mg/kg, i.p.), labyrinthectomy was performed in rats using an operating microscope. The tympanic membrane, malleus, and incus were removed by the retroauricular approach. The stapes crusa were fractured and then the stapes footplate was removed to open the oval window. A small opening was established by drilling the bony horizontal semicircular canal. After aspiration of labyrinth fluid from the oval window, the membranous